Singlet oxygen plays a key role in the toxicity and DNA damage of nanometric TiO2 to human keratinocytes

Singlet oxygen plays a key role in the toxicity and DNA damage caused by nanometric TiO_2 in human keratinocytes

[Nanoscale, 2013, 5, 6567-6576 DOI: 10.1039/c3nr01191g]

Singlet oxygen plays a key role in the toxicity and DNA damage caused by nanometric TiO_2 in human keratinocytes†

Ivana Fenoglio,*[a] Jessica Ponti,*[b] Elisa Alloa,[b] Mara Ghiazza,[a] Ingrid Corazzari,[a] Robin Capomaccio,[b] Diana Rembges,[b] Simonetta Oliaro-Bosso[c] and François Rossi[b]

Nanometric TiO_2 has been reported to be cytotoxic and genotoxic in different in vitro models when activated by UV light. However, a clear picture of the species mediating the observed toxic effects is still missing. Here, a nanometric TiO_2 powder has been modified at the surface to completely inhibit its photo-catalytic activity and to inhibit the generation of all reactive species except for singlet oxygen. The prepared powders have been tested for their ability to induce strand breaks in plasmid DNA and for their cytotoxicity and genotoxicity toward human keratinocyte (HaCaT) cells (100–500 μg mL^{-1}, 15 min UVA/B exposure at 216–36 mJ m^{-2} respectively). The data reported herein indicate that the photo-toxicity of TiO_2 is mainly triggered by particle-derived singlet oxygen. The data presented herein contribute to the knowledge of structure–activity relationships which are needed for the design of safe nanomaterials.

1 Introduction

The rapid diffusion of nanotechnological products in the market raises concerns about the possible adverse effects on human health caused by those materials which contain nano-particles. The potential toxicity of the nanoparticles to humans is, in fact, the subject of a large debate.[1–4] There are two different approaches for the safe development of nanotechnology: the assessment and the management of the risk associated with the exposure to each kind of nanoparticle or the set-up of strategies for the design of safe (or safer) nanomaterials. The knowledge of defined structure–activity relationships is a prerequisite for the latter approach.

Titanium dioxide (titania, TiO_2) is largely used as both a micrometric and nanometric size powder. Micrometric TiO_2 has an application as the white pigment in paint, and also in composites, cosmetics, food and pharmaceutical products. In the nanometric form, TiO_2 loses the ability to scatter visible light but retains its UV scattering and adsorption activity. For this reason this material is widely used in transparent UV-filters.[5–7] Due to the high surface area, TiO_2 nanometric powders also find applications as photo-catalysts. In fact, when TiO_2 particles are irradiated by UV light, charge separation takes place in the bulk producing both electrons (e^-) and holes (h^+) which migrate to the surface of the solid promoting reductive and oxidative reactions, respectively.[8] When the activation occurs in aqueous media, large amounts of several reactive oxygen species (ROS), e.g. hydroxyl radicals ($HO^{\cdot}$), superoxide radical anions ($O_2^{\cdot -}$) and singlet oxygen ($^1O_2$), are produced. In high concentrations these species are highly toxic to living organisms including mammalian cells.[9,10]

Several studies report that TiO_2 nanoparticles are rapidly internalized by cells.[11–15] When irradiated with UVA/B radiation (280–400 nm), TiO_2 nanoparticles induce cell death and DNA damage in several different models.[16–22] Particle-derived ROS appear clearly involved in the mechanism of toxicity since, in absence of illumination, the adverse effects are much lower than under irradiation.[12,23] However other deleterious effects, like a reduction in keratinocyte proliferation and the alteration of calcium homeostasis, have been observed in the dark.[12,23] Among the different ROS, hydroxyl radicals (HO_) are generally considered to be the most reactive ones and therefore the induction of oxidative damage is often related to this radical species.[16,17,24] Conversely the role of singlet oxygen ($^1O_2$) has been scarcely

[a]Dipartimento di Chimica, "G. Scansetti" Interdepartmental Center for Studies on Asbestos and other Toxic Particulates and Interdepartmental Center for Nanostructured Interfaces and Surfaces, University of Torino, via P. Giuria 7, 10125- Torino, Italy. E-mail: ivana.fenoglio@unito.it; Fax: +39 116707577; Tel: +39 116707506

[b]European Commission, Joint Research Centre, Institute for Health and Consumer Protection, (EC-JRC-IHCP), via Fermi 2749, 21027 ISPRA (Va), Italy. E-mail: jessica.ponti@jrc.ec.europa.eu; Fax: +39 0332 78 5787; Tel: +39 0332 78 5793 [c]Dipartimento di Scienza e Tecnologia del Farmaco, University of Torino, via P. Giuria 9, 10125-Torino, Italy. E-mail: simona.oliaro@unito.it; Fax: +39 116707663; Tel: +39 116707664

† Electronic supplementary information (ESI) available: (1) ζ potential as a function of pH; (2) crystalline phase (XRD); (3) UV-Vis shielding capacity; (4) evaluation of particle size (CPS); (5) the UVA/B irradiation system used in the cellular experiments. See DOI: 10.1039/c3nr01191g

investigated. This species is not a radical, but similarly to them it can induce oxidative damage. In fact it reacts with unsaturated fatty acids leading to peroxides which may in turn activate the lipoperoxidation process.[25] Singlet oxygen may also react with nucleotides leading to several oxidative products.[26]

To get an insight into the role of singlet oxygen in the toxicity of irradiated TiO_2, a set of three samples of nanometric titanium dioxide, modified at the surface to modulate their ability to generate ROS while keeping constant their other properties, have been prepared and tested for their cyto- and genotoxicity toward human keratinocytes.

2 Results

2.1 Preparation and characterization of the TiO_2 samples

A commercial powder (Aeroxide P25, Degussa) was chosen to model the highly photo-active TiO_2 ($T_{A/R}$). This powder, which has been used and characterized in several studies,[27,28] is produced from the hydrolysis of $TiCl_4$ at high temperature and is composed of anatase that has been partially converted to rutile.

The surface of this sample was firstly modified to reduce its photo-activity by a protocol previously described,[29,30] based on the thermal decomposition of ethylene glycol ($T_{A/R}$–C). This sample, exhibiting at the surface carbonaceous and carbonate/carboxylate-like species, has been shown to be inactive in the generation of most ROS except for singlet oxygen.[29,30] $T_{A/R}$ was further modified by a wet impregnation–calcination protocol with $Fe(NO_3)_3$ as described in the Experimental section ($T_{A/R}$–Fe). Transition-metal-doped TiO_2, particularly with iron, is widely studied since doping with transition metals may enhance the photo-catalytic activity of TiO_2 in the visible light region.[31,32] The photo-catalytic efficiency of iron doped TiO_2 is dependent upon the synthetic route and loading. In fact, while an enhancement of the photocatalytic activity is observed for low loadings,[33,34] high loadings of Fe^{3+} ions have a detrimental effect since they serve as recombination centres for the photo-induced charge carriers.[35–39] Here, a treatment leading to the grafting at the surface of a large amount of iron ions (12.4%) was performed to suppress the generation of reactive species.

The main physico-chemical properties of the pristine and modi fied samples are summarized in Table 1. Both the specic surface area[11,40] and crystalline phase[20,28,41] have been shown to modulate the reactivity and toxicity of TiO_2. In the present case, the three samples prepared exhibited a similar abundance of the anatase and rutile crystalline phases (see ESI†) and a specic surface area (SSA) in the same range. A slight decrease in the SSA was observed in the treated samples as a consequence of the thermal treatment performed during the modification, which is possibly due to the partial sintering of the particles. Another important parameter is the charge of the surface, which arises from the presence of dissociated or protonated functional groups.[42] The surface charge was shown to modulate the cell response[43] as well as the stability of the nanoparticle suspensions. In fact, the existence of repulsion forces among the nanoparticle surface inhibits their agglomeration. The extent of the surface charge may be estimated by measuring the ζ potential in water, i.e. the potential measured across the double layer of ions around the particles.[42] By measuring the ζ potential as a function of pH the point of zero charge (PZC) may also be determined (see ESI†). Both treatments performed shifted the ζ potential curves and the PZC toward lower pH values suggesting the higher acidity of the surface of the modified samples. As a result, at neutral pH, the ζ potential values of $T_{A/R}$–Fe and $T_{A/R}$–C were slightly more negative than that of the pristine sample (see ESI† and Table 1). The shift of the PZC of $T_{A/R}$–Fe toward lower pH values excludes the possibility of the coating masking the surface since the PZCs of iron oxides are reported to be at much higher values (7–9.5).[44]

The samples have also been analyzed by diffuse UV-Vis re flectance (see ESI†). The pristine material shows the typical spectrum of TiO_2 with an intense absorption in the UV region (l < 400 nm). $T_{A/R}$–C shows the same behaviour as bare TiO_2 in the UV region. However, a further continuous absorption in the entire visible light region is observed which can be ascribed to the presence of the carbonaceous species at the surface.[30] An enhanced absorbance in the visible region is observed also for $T_{A/R}$–Fe. In this case, two broad bands centred at *ca.* 415 and 500 nm related to the excitation of 3d electrons and to d–d transitions respectively[39] were detected.

2.2 Photo-induced ROS generation

Electron paramagnetic resonance spectroscopy (EPR)/spin trapping is a powerful technique which has been widely used to evaluate the ability of TiO_2 to generate free radical species.[45,46] Here, specific spin trapping molecules and experimental conditions were used to trap the primary photo-generated species i.e. the superoxide radicals ($O_2^{\cdot-}$)and hydroxyl radicals ($HO^{\cdot}$). A filtered UV lamp (see Experimental section) was used to model real daylight exposure.

Table 1 The physico-chemical properties of the TiO_2 samples; nd ¼ not determined

Sample	Crystalline phases	Speci c surface area ($m^2\ g^{-1}$)	Elemental composition (%)	Primary particle size (nm)	Aggregates mean size (nm)/PdI	ζ potential in water, pH 7.4
T						
$T_{A/R}$	Anatase–rutile	52.6	TiO_2 > 99.6[a]	25.20 _ 0.20[a]	89/1.60	_21.5
$T_{A/R}$–C	Anatase–rutile	49.9	99 TiO_2, 1 carbon[b]	nd	108/1.64	_29.9
$T_{A/R}$–Fe	Anatase–rutile hematite (traces)	38.8	87.6 TiO_2, 12.4 (Fe_2O_3)	nd	92/2.13	_36.5

[a] Gerlo*ff* et al. 2011.[28] [b] Corazzari et al. 2012.[30]

Superoxide anion radicals ($O_2^{\cdot-}$) are generated from the reduction of oxygen by photo-generated electrons (eqn 1) while hydroxyl radicals ($HO^{\cdot}$) are formed in the reaction of the photo-generated holes with water (eqn 2).

$$e^- + O_2 \rightarrow O_2^{\cdot-} \quad (1)$$

$$h^+ + H_2O \rightarrow HO^{\cdot} + H^+ \quad (2)$$

The photo-generated holes may also directly oxidize organic molecules. The occurrence of this reaction was monitored using sodium formate as the model molecule. In this case, carboxylate radicals ($CO_2^{\cdot-}$) are formed (eqn 3).

$$h^+ + HCO_2^- \rightarrow CO_2^{\cdot-} + H^+ \quad (3)$$

As previously reported,[30] the pristine sample was active in all reactions (spectra a in Fig. 1A–C) while no hydroxyl or super-oxide radicals were detected for either $T_{A/R}$–Fe or $T_{A/R}$–C (spectra b, c, Fig. 1A and B). The amount of carboxylate radicals largely decreases for the modified samples although traces of the signal were detected (spectra b, c, Fig. 1C) suggesting that the residual oxidizing sites remained stabilized at the surface.

The powders have also been tested for their ability to generate singlet oxygen ($^1O_2$). The mechanism of the generation of this reactive species is poorly known. Some authors suggested that the formation of singlet oxygen occurs by a recombination process as described by eqn 4, which leads to the transfer of excess energy to oxygen, thus promoting it to the excited state.[47]

$$h^+ + O_2^{\cdot-} \rightarrow {}^1O_2 \quad (4)$$

The occurrence of this reaction has been evaluated using the spin probe 4-oxo-TMP which reacts with singlet oxygen leading to the formation of a paramagnetic nitroxide which is detectable by EPR (Fig. 1D).[45,48] In this case, singlet oxygen was detected only for the pristine sample and for $T_{A/R}$–C, while the sample modified with iron ($T_{A/R}$–Fe) was completely inactive.

The generation of singlet oxygen was further confirmed by spectrophotometry by using a colored dienic molecule (rubrene) as the probe. Singlet oxygen reacts with the orange rubrene in a Diels–Alder [4 + 2] cycloaddition producing a colorless endoperoxide.[49,50] The amount of singlet oxygen generated is thus inversely proportional to the absorbance measured from the supernatant of the solution in the 400–600 nm range after contact with TiO_2 and exposure to simulated sunlight.

In Fig. 2, the spectra of the solution of rubrene irradiated with the simulated solar light in the presence of each TiO_2 sample is compared with the spectra of the solution irradiated in the absence of the powders. A dramatic decrease in the intensity of the peaks typical of rubrene (l_{max} ¼ 524, 490, 461 and 431 nm) was observed in the presence of $T_{A/R}$ and $T_{A/R}$–C only.

The experiments were also performed in the dark: under this condition, the surface reactivity was almost totally suppressed albeit traces of the free radical species were detected for $T_{A/R}$ and $T_{A/R}$–C (data not shown).

2.3 Direct damage of plasmid DNA

Several studies have reported the ability of irradiated TiO_2 to directly damage DNA.[17,19,24,51] Here, the potential of $T_{A/R}$, $T_{A/R}$–Fe and $T_{A/R}$–C to cause direct oxidative damage to DNA was evaluated by incubating the powders with supercoiled plasmid double-stranded DNA (SC). The occurrence of strand breaks leads to the conversion of the SC form into open circular (OC) and linear (L) forms (Fig. 3) which was confirmed by incubating the plasmid DNA with the endonuclease enzyme EcoRI, both in the absence and presence of a high concentration of ethidium bromide, which partially inhibits the DNA cutting by EcoRI, causing the formation of OC DNA[52] (Fig. 3, lanes 2 and 3).

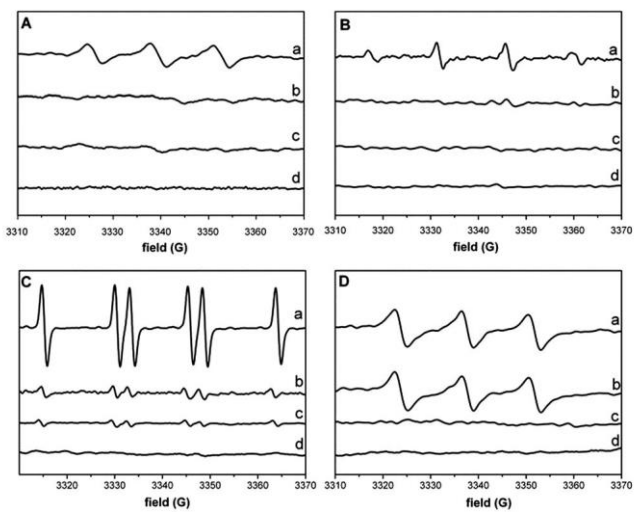

Fig. 1 The generation of free radicals under simulated solar light conditions detected by EPR/spin trapping or probing techniques by (a) $T_{A/R}$, (b) $T_{A/R}$–C, (c) $T_{A/R}$–Fe and (d) control (no powder); (A) generation of superoxide radicals ($O_2^{\cdot-}$), (B) generation of hydroxyl radicals (HO), (C) generation of carboxylate radicals (_ $CO_2^{\cdot-}$), (D) generation of singlet oxygen ($^1O_2$).

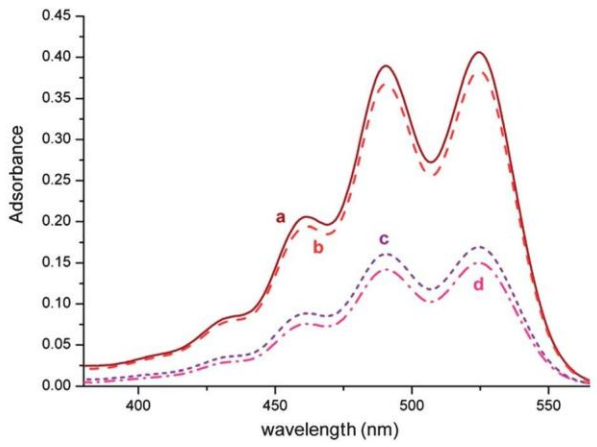

Fig. 2 The oxidation of rubrene by photo-generated singlet oxygen ($^1O_2$) under simulated solar light conditions. (a) Rubrene solution (no powder), (b) $T_{A/R}$–Fe, (c) $T_{A/R}$–C, (d) $T_{A/R}$.

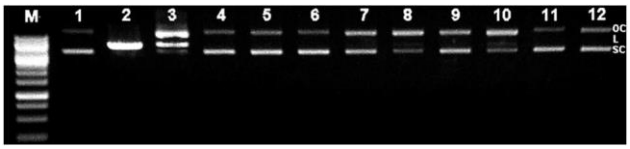

Fig. 3 Photo-induced damage to double stranded supercoiled plasmid DNA. Lane (1) native DNA, lane (2) DNA + EcoRI, lane (3) DNA + EcoRI + ethidium bromide, lanes (4) and (5) DNA exposed for 10 and 20 minutes to simulated solar light, lane (6) DNA + $T_{A/R}$ in the dark, lane (7) and (8) DNA + $T_{A/R}$ exposed for 10 and 20 minutes to simulated solar light, lanes (9) and (10) DNA + $T_{A/R}$–C exposed for 10 and 20 minutes to simulated solar light, lanes (11) and (12) DNA + $T_{A/R}$–Fe exposed for 10 and 20 minutes to simulated solar light.

The irradiation for 10 and 20 minutes of the plasmid DNA incubated with the $T_{A/R}$ powder caused a significant increase in the amount of the OC form (Fig. 3, lanes 7 and 8), with respect to plasmid DNA irradiated in absence of powder (Fig. 3, lanes 4 and 5). This effect is related to the photo-activation of the pristine powder ($T_{A/R}$), since in the dark it was not observed (Fig. 3, lane 6). Incubation of the plasmid DNA with the $T_{A/R}$–C powder induces the formation of a supercoiled/open circular DNA ratio which is similar to that of $T_{A/R}$ (Fig. 3, lanes 9 and 10) suggesting that strand breakage occurs through singlet oxygen induced oxidative damage. As expected, the inactive $T_{A/R}$–Fe powder did not induce any effect on DNA (Fig. 3, lanes 11 and 12)

2.4 Agglomeration in the cell media

The size of the $T_{A/R}$, $T_{A/R}$–Fe and $T_{A/R}$–C particles was measured by centrifugal sedimentation (CS) in water, serum-free cellular media and cellular media complemented with 10% of serum and at time 0, after 15 minutes of exposure to artificial sunlight and after 2 hours at 37 °C in the dark (see ESI†).

The pristine material was polydispersed under all conditions as suggested by the high polydispersity indexes (PdI, see ESI†) thus confirming what has been previously found.[28] The mean size of the particles in water was 89 nm, which is larger than the mean size of the crystallites (25 nm) because of the presence of stable aggregates. The modified samples exhibited a similar mean size in water and a similar polydispersity degree (see ESI†). When the particles were dispersed in serum-free media an increase in the mean particle size was observed which is likely due to the high ionic strength of the media and the possible masking of the surface by the cell media components (see ESI†). In the presence of serum, the size of the agglomerates decreased following the stabilizing effect of the proteins interacting with the surface.[28] The exposure of the suspension to simulated sunlight induced an increase in the agglomerate size which is probably due to the modification of the hydrophilic degree of the surface.[53] However this effect was similar for all samples in the cellular media.

2.5 Cytotoxicity toward human keratinocyte HaCaT cells

Cytotoxicity has been measured in the dark and with UVA/B radiation. Short times of irradiation (15 min) and incubation (2 h) were chosen to avoid effects not related to photo-activation which have been observed for longer times of incubation in other studies.[12,23] The tailor made UVA/B exposure cabinet used (see Experimental section and ESI†) simulates a realistic UVA/B exposure occurring on a summer day. The powders exhibited different activities on human keratinocyte HaCaT cells. While $T_{A/R}$–Fe did not show any cytotoxic effect (Fig. 4A), $T_{A/R}$ and $T_{A/R}$–C showed statistically significant cytotoxicities with respect to the control at both concentrations tested. A clear dose-dependent inhibition of the colony forming efficiency (CFE) by the $T_{A/R}$ and $T_{A/R}$–C samples was observed only under UVA/B radiation, while in the dark, no statistical significant effect was observed even after 2 h of exposure to the powders (Fig. 4B)

2.6 Genotoxicity toward human keratinocyte HaCaT cells

In order to investigate the genotoxic potential of the powders, the induction of DNA strand breaks was evaluated by means of the comet assay, while the formation of oxidized purines and pyrimidines was evaluated using the Fpg and Endo III enzymes, respectively (Fig. 5).

The results clearly showed a genotoxic effect induced by $T_{A/R}$ and $T_{A/R}$–C only in the HaCaT cells exposed to UVA/B radiation, where the induction of DNA strand breakage and an increase in the amount of oxidized purines and pyrimidines were observed. Conversely $T_{A/R}$–Fe did not significantly affect DNA (Fig. 5 A), however there was a small increase in the amount of oxidized purine observed for this sample.

Interestingly, the DNA damage was more predominant at purine sites recognized by the Fpg enzyme. However, we cannot exclude the possibility that this effect was due to the adsorption or interaction of the TiO_2 NPs with the Endo III enzyme leading to a lower availability and a reduction of its activity.[54]

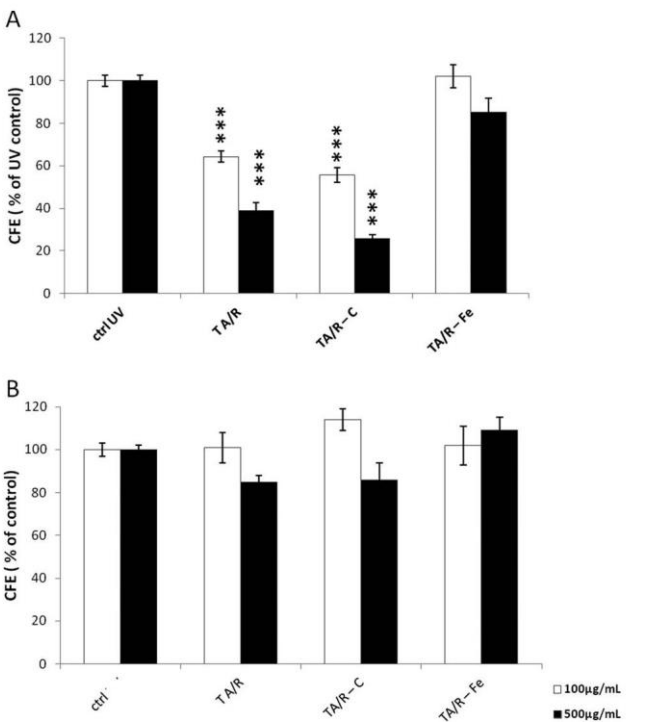

Fig. 4 The effect of the $T_{A/R}$, $T_{A/R}$–C, $T_{A/R}$–Fe samples on the colony forming efficiency (CFE) of HaCaT cells (A), with 15 min UVA/B radiation exposure, and (B) under standard cell culture conditions and 2 h of exposure. The results are expressed as CFE% of the control under UVA/B radiation exposure (A) and of the negative control under standard cell culture conditions (dark, B). ***P < 0.001

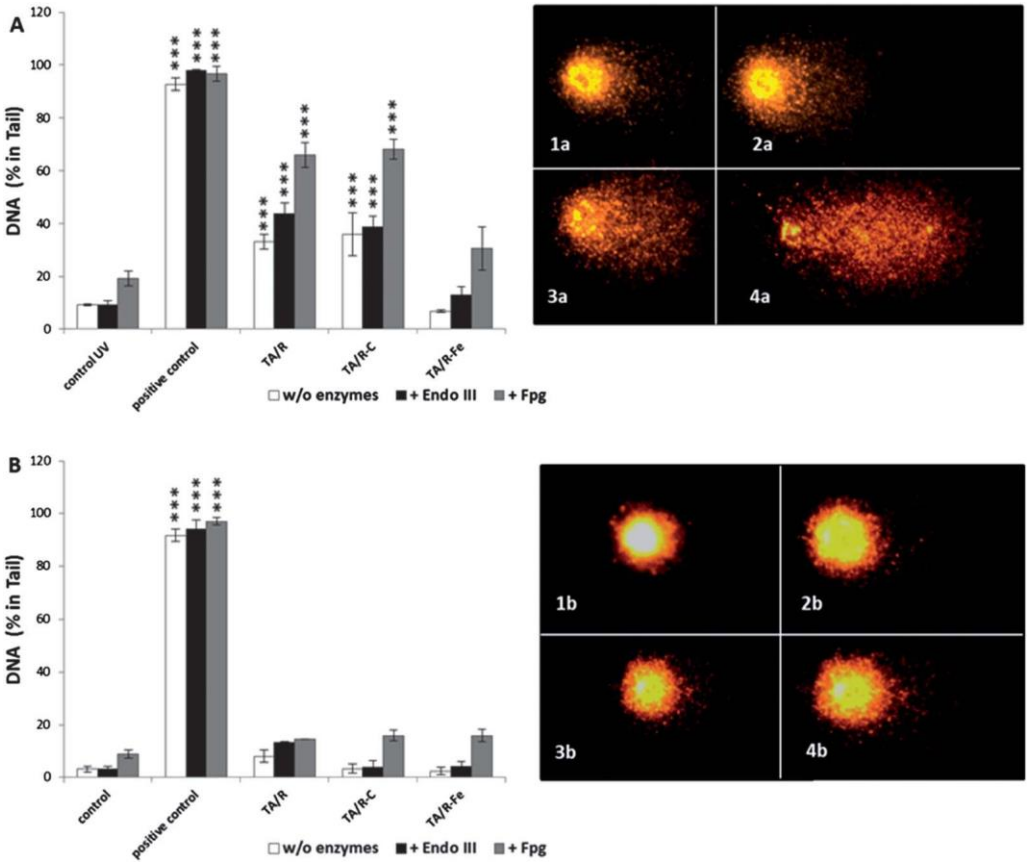

Fig. 5 Primary DNA damage (without enzymes), oxidative pyrimidine (+ Endo III) and purine (+ Fpg) DNA damage, measured by a comet assay in HaCaT cells after exposure to $T_{A/R}$, $T_{A/R}$–C and $T_{A/R}$–Fe. (A) Under simulated solar light with 15 min of exposure. (B) Under standard cell culture conditions with 2 h of exposure. The results are expressed as % of DNA in the tail. ***P < 0.001. The images on the right are representative pictures of primary DNA damage (a) with exposure to UVA/B radiation and (b) in the dark: (1) primary DNA damage (without enzymes) in cells (no powders), (2) primary DNA damage in cells exposed to $T_{A/R}$, (3) oxidative pyrimidine DNA damage (+ Endo III) in cells exposed $T_{A/R}$, (4) oxidative purine DNA damage (+ Fpg) in cells exposed to $T_{A/R}$.

3 Discussion

The use of sunscreen is highly recommended to avoid UV-induced skin ageing and pigmentation and, more importantly, to reduce the incidence of skin cancer.[7,55,56] A large part of sunscreens contains combinations of chemical and physical UV-filters (TiO_2 or ZnO), in particular when high sun protection factors (SPF) are needed.[57] Due to the widespread use of sunscreens several studies have focused on determining the safety of the TiO_2 and ZnO nanoparticles. The data reported here and in previous studies clearly show that photo-active TiO_2 triggers cytotoxic and genotoxic effects in several in vitro models.[16–22] At the same time, the data currently available indicate that nanometric TiO_2 does not penetrate beyond the stratum corneum or hair follicles into the viable keratinocytes of healthy skin and therefore probably does not pose a risk to consumer health.[6,7,55–60] Nevertheless, studies on the possible penetration following long term exposure and on damaged skin (psoriasis, acne, and burning) are lacking or are still in the early stages.[7,61–64] On the other hand, photo-reactive physical UV-filters contribute to decreasing the photo-stability of the sunscreen, since photo-generated ROS are able to degrade the organic ingredients, including the chemical filters.[57]

Nanometric titania is approved as a UV-filter in cosmetics regardless of its form and reactivity (Cosmetics Directive 76/768/EEC, http://www.fda.gov), however as a matter of fact commercial TiO_2 nanopowders for cosmetic applications are always coated with inorganic and/or organic coatings.[65,66] Several coatings have been shown to be efficient in inhibiting the reactivity of titania[65,66] but in other cases coated commercial powders were found to be photo-reactive.[20,45,67,68] In particular, Buchalska and co-workers recently found that the TiO_2 nanoparticles found in commercial sunscreens may generate singlet oxygen.[69]

The agreement between the results obtained here on plasmid DNA and on the keratinocytes (Table 2), as well as the detection of oxidized nucleotide bases in damaged keratinocytes, confirms a mechanism of acute toxicity involving the direct oxidative damage of DNA by photo-generated ROS, a mechanism which has been previously suggested by other authors.[17–21] The inertness on both the plasmid DNA and the keratinocytes of the photo-inactive iron-doped sample further confirms this finding.

Table 2 A comparison of the data obtained in cell-free and cellular tests

Sample	Photo-generated ROS	Direct damage in plasmid DNA	Cytotoxicity	Genotoxicity
$T_{A/R}$	$HO^{\cdot}$, $O_2^{\cdot-}$, $^1O_2$	Yes	Yes	Yes
$T_{A/R}$–C	$^1O_2$	Yes	Yes	Yes
$T_{A/R}$–Fe	—	No	No	No

In the dark, no effects were observed for any samples. This finding excludes the possibility that the toxic effects observed were due to mechanisms other than photo-activation.

$T_{A/R}$–C, which generates only singlet oxygen, induced strand breaks to plasmid DNA similar to that found with the pristine sample, and elicited similar genotoxic effects on keratinocytes. This clearly demonstrates the major role of photo-generated singlet oxygen in the genotoxicity of TiO_2 toward human keratinocytes. Therefore, based on our results, photo-generated free singlet oxygen may be considered a marker of potential toxicity of TiO_2 based UV-filters.

4 Experimental

4.1 Titanium dioxide samples

The rutile–anatase TiO_2 (Aeroxide P25), hereafter named $T_{A/R}$, was purchased by Evonik, (Essen, Germany).

The carbon-modified powder (hereafter named $T_{A/R}$–C) was obtained following a protocol previously employed by some of us.[30] 1 g of $T_{A/R}$ was suspended overnight with continuous stirring in a 2.5 M ethylene glycol aqueous solution. The powder was successively filtrated and dried at 343 K and then heated in air at 573 K for 30 min with a heating rate of 10 K min^{-1} in a quartz tube in the presence of 20 mbar of oxygen. The modified powder was then washed with water to remove any molecules that were weakly bound to the surface.

The iron-modified powder ($T_{A/R}$–Fe) was prepared using the so-called "wet impregnation" method, which is widely used for the preparation of heterogeneous catalysts. 1 g of titanium dioxide was suspended in 3 mL of an aqueous solution of $Fe(NO_3)_3$, 0.2 M. The suspension was dried at 313 K for 24 h in order to allow intimate contact between the iron ions and titania support. The procedure was then repeated to ensure a better impregnation. The product obtained was washed three times with distilled water to eliminate any iron not firmly bound to the surface. The samples were then dried and subsequently calcinated at 873 K for 16 h.

4.2 Determination of the specific surface area

The specific surface area (SSA) of both the pristine and modified samples was measured by means of a Brunauer–Emmett–Teller (BET) method based on N_2 adsorption at 77 K (ASAP 2020 Micrometrics, Norcross, GA).

4.3 Elemental composition

The elemental composition was evaluated using an EDAX Eagle III energy dispersive micro-XRF spectrometer equipped with a Rh X-ray tube and a polycapillary exciting a circular area which was nominally 30 μm in diameter. Data collection occurred at each point for 200 s detector live time, with X-ray tube settings adjusted for 30% dead time. About 1 _ 10^6 Cps were counted per scan. At least 4 points were collected for each sample.

4.4 Diffuse reflectance UV-Vis spectroscopy (DR UV-Vis)

Spectra were recorded using a Varian Cary 5 spectrometer using Cary win-UV/scan software.

4.5 Measurement of ζ potential

The ζ potential values were obtained by means of electrophoretic light scattering (ELS) (Zetasizer Nano-ZS, Malvern Instruments, Worcestershire, U.K.) on powders suspended (50 mg L^{-1}) in ultrapure water (Milli-Q) after adjusting the pH step by step with the addition of 0.1 M NaOH or 0.1 M HCl.

4.6 Irradiation equipment

In cell-free tests the irradiation experiments were performed with a 500 W mercury/xenon lamp (Oriel Instruments) equipped with an IR water filter to avoid the overheating of the suspensions. Simulated solar light was obtained by applying a 400 nm cut-off filter that let about 5% of the UV light pass in the UVA region. The light irradiance in the UVA region was measured by a Deltahom (Caselle di Selvazzano, Padova, Italy) instrument equipped with a detector operating in the UVA range (315–400 nm). An irradiance of 8.4 _ 10^{-2} W m^{-2} was measured in all the experiments.

In cellular tests, a tailored UV exposure cabinet equipped with an adjustable ULTRALUX 300 W lamp ensured a homogeneous exposure inside the 6-well plate. The lamp was checked by a Diode Array System for Laboratory measurements (DAY-SYLAB SP-J1009, Schreder CMS).[70] The exact exposure position for the 6-well plate has been selected on the basis of UVA/B dose measurements (see ESI†). The applied radiation to the cells in the culture plate was about 0.4 W m^{-2} for UVB (280–315 nm) and 2.7 W m^{-2} for UVA (315–400 nm) (see ESI†).

A 3.1 W m^{-2} total UVA/B radiation roughly represents the intensity of sunbathing in July/August around noon in central Europe. An exposure duration of 15 minutes was selected in order to simulate a realistic UV exposure occurring in summer during common daily human activities.

4.7 The generation of free radicals

The generation of radical species was monitored by electron spin resonance (EPR) spectroscopy (Miniscope 100 EPR spectometer, Magnettech, Berlin, Germany) associated with the spin

trapping technique using DMPO (5,5-dimethyl-1-pyrroline-N-oxide, Alexis Biochemicals, San Diego, CA) and PBN (N-tert-butyl-a-phenylnitrone, Sigma-Aldrich, St. Louis, MO) as spin trapping agents. The generation of $^1O_2$ was monitored by EPR spectroscopy employing 4-oxo-TMP (2,2,6,6-tetramethyl-4-piperidone, Sigma-Aldrich) as a spin probing agent. All the other reagents employed were from Sigma-Aldrich. For the aqueous solutions ultrapure Milli-Q water (Millipore, Billerica, MA) was used. All the experiments were performed on a per area basis.

1. Superoxide radicals. The amount corresponding to 1.4 m^2 of exposed surface area of the powders were suspended in 0.8 mL of a 20 mM PBN solution in cyclohexane, and the suspension was irradiated with simulated solar light and constantly stirred. The EPR spectra were recorded using a sample suspension (50 mL) withdrawn after 60 min.

2. Hydroxyl radicals. The amount corresponding to 1.4 m^2 of exposed surface area of the powders were suspended in 1.25 mL of a buffer solution (100 mM potassium phosphate buffer pH 7.4) containing DMPO (35 mM). The suspension was irradiated with simulated solar light and constantly stirred. The EPR spectra were recorded using a sample suspension (50 mL) withdrawn after 60 min.

3. Carboxylate radicals. The amount corresponding to 1.4 m^2 of exposed surface area of the powders were suspended in 0.5 mL of a buffer solution (125 mM potassium phosphate buffer pH 7.4) containing DMPO (88 mM) and sodium formate (1 M). The suspension was irradiated with simulated solar light and constantly stirred. The EPR spectra were recorded using a sample suspension (50 mL) withdrawn after 60 min.

4. Singlet oxygen. The amount corresponding to 1.4 m^2 of exposed surface area of the powders were suspended in 1 mL of a 50 mM solution of 4-oxo-TMP in cyclohexane. The suspension was irradiated with simulated solar light and constantly stirred. The EPR spectra were recorded using a sample suspension (50 mL) withdrawn after 10 min. The capability of the powders to generate singlet oxygen was also monitored by spectrophotometry employing rubrene as a probe molecule. A 0.15 M solution was prepared dissolving rubrene in acetonitrile–n-butanol (5 : 1). The mixture was continuously stirred in the dark to prevent its photoxidation. The amount corresponding to 0.1 m^2 of exposed surface area of the powders were suspended in 2 mL of the rubrene solution in a quartz vial. The suspension was irradiated with simulated solar light and constantly stirred. After 5 min of incubation the powder was removed by centrifuging the suspension (1200 RCF). The supernatant was filtered through PTFE membrane filters (Advantec, Toyo Roshi Kaisha, Japan; pore diameter 0.20 μm) and the absorbance (l_{max} ¼ 525 nm) was measured by means of a Uvikon UV-Vis spectrophotometer (Kontron Instruments Inc., Everett, MA). A rubrene solution irra-diated in the same conditions but in the absence of the powder was employed as a blank.

4.8 Oxidative damage to plasmid DNA

pYES2 plasmid DNA (Invitrogen, Italy) was used as the model. The DNA strand breaks were detected by agarose (1%) gel electrophoresis. All experiments were performed using _0.2 mg of powder (pristine and modified) which was suspended in 30 μL of Milli-Q water and then vortexed. To this suspension 3 μL of DNA solution (100–150 ng mL^{-1}) were added and then exposed to a simulated solar light (see above) for different times (0, 10 and 20 minutes). The control was DNA irradiated for the same time in the absence of any powder in order to exclude a direct damage to this molecule. After irradiation, the suspension was centrifuged and the supernatant used for gel electro-phoresis. DNA bands were stained and visualized with ethidium bromide (Promega, Italy).

EcoRI nicking was done using EcoRI (20 units per μL) from New England Biolabs, Italy. _3 μg of the supercoiled plasmid DNA pYES2 were incubated with 50 units of the EcoRI enzyme in 100 mM Tris–HCl (pH 7.5), 50 mM NaCl, 10 mM $MgCl_2$ and 0.025% Triton X-100, both in the absence or in the presence of 200 μg mL^{-1} ethidium bromide (final volume of reaction 15 μL). The reaction was carried out at 26 °C over 16 hours. 0.5 μL of the sample was loaded on a 1% agarose gel.

4.9 The preparation of the nanoparticle suspensions for cell testing.

10 mg of the TiO_2 powders (pristine and modified: $T_{A/R}$, $T_{A/R}$–C and $T_{A/R}$–Fe) were weighed and suspended in 1 mL of Milli-Q sterile water. Samples were sonicated in an ultrasonic bath for 15 min under controlled temperature conditions. Suspensions were then diluted in complete cell culture medium composed of DMEM high glucose with or without phenol red (Invitrogen, Italy), 10% (v/v) Fetal Clone II serum (Hyclone, Celbio, Italy) and 1% (v/v) pen–strep (Invitrogen, Italy) to reach final testing concentrations of 100 and 500 μg mL^{-1}.

4.10 Size measurement of particles and agglomerates in cell media

The nanoparticle size distribution was measured by centrifugal sedimentation (sucrose gradient 8.7–31.6%; Disc Centrifuge model DC24000, CPS Instruments Europe, The Netherlands), assuming that the density of $T_{A/R}$–Fe and $T_{A/R}$–C were the same as that of $T_{A/R}$, and the peak of the weight of the particles was automatically detected. Pristine and modified TiO_2 powders were prepared as described above and diluted in Milli-Q water, complete culture medium and serum-free culture medium reaching the concentration of 100 μg mL^{-1}.

The size has been evaluated under three conditions: at time 0, after 15 min with irradiation from an Ultralux 300 W lamp installed in an irradiation chamber[56] and after 2 hours of incubation under standard cell culture conditions (5% CO_2, 95% humidity, 37 °C).

4.11 Cell culture conditions

Human keratinocyte cells (HaCaT) were originally supplied by the German Cancer Research Center (Germany). Experimental cultures were prepared from deep-frozen stock vials and maintained in culture in a sub-confluent state (not more than 70%). HaCaT cells were cultured in DMEM high glucose (Invitrogen, Italy) to which 10% (v/v) Fetal Clone II serum (Hyclone,

Celbio, Italy) and 1% (v/v) pen–strep (Invitrogen, Italy) were added, and maintained under standard conditions (37 °C, 5% CO_2 and 95% humidity, Heraeus incubator, Germany).

4.12 Cytotoxicity assay

The colony forming efficiency (CFE) assay was carried out exposing cells to 100 and 500 μg mL^{-1} of $T_{A/R}$, $T_{A/R}$–C and $T_{A/R}$–Fe for 2 h under standard cell culture conditions (5% CO_2, 95% humidity, 37 °C) under dark conditions and for 15 min under UVA/B radiation exposure to assess the cytotoxicity of the $T_{A/R}$, $T_{A/R}$–C and $T_{A/R}$–Fe suspensions. HaCaT cells were seeded at a density of 200 cells per dish (60 x 15 mm Petri dish, Corning, Costar, Italy) in 3 mL of complete culture medium for the dark conditions and at the same density but in 2.5 mL per well in a 6-well plate (Falcon, Italy) for the cells exposed to UVA/B radiation. After 24 h, the medium was changed with the standard complete cell culture medium for the samples in the dark and with complete culture medium without phenol red for the samples exposed to UVA/B radiation. Aliquots of the $T_{A/R}$, $T_{A/R}$–C and $T_{A/R}$–Fe suspensions were added to each dish or well obtaining the testing concentrations of 100 and 500 mg mL^{-1}. After exposure the medium was changed with complete fresh culture medium that was renewed twice per week. After 10 days, the cells were fixed for 20 min with a 3.7% (v/v) formaldehyde solution (Sigma, Milan, Italy) in phosphate buffer solution (PBS) (1_, GIBCO, Italy). Dishes were stained for 30 min with a 10% (v/v) Giemsa solution (GS-500, Sigma, Italy) in ultrapure water. Colonies were scored with a Gelcount colony counter (Oxford Optronix). Each experiment included a negative control (untreated cells), a positive control that induced complete cell death (cells exposed to sodium chromate 1000 μM, Sigma, Italy) and a control exposed to UVA/B radiation (untreated cells but exposed to UVA/B radiation). The results are expressed as the CFE (% of the control) for the dark conditions or the CFE (% of the control) for the samples exposed to UVA/B radiation (CFE = average of treatment colonies/average of control colonies ×100). The corresponding standard error mean was calculated for at least 3 independent experiments and at least 3 replicates for each experimental point (standard error mean= SD/√number of replicates). The statistically significant differences were calculated by the one-way ANOVA analysis (GraphPadPrism4 statistical so ware, GraphPad Inc., CA, USA).

4.13 The comet assay

250 000 cells (6-well plate, Falcon, Italy) were seeded in 3 mL of complete culture medium in each well. After 24 h, the medium was changed with complete cell culture medium for the cells in the dark and with complete culture medium without phenol red for the cells exposed to UVA/B radiation. Cells were exposed as described for the CFE assay. Each experiment included a negative control (untreated cells), a positive control (cells exposed to 100 μM H_2O_2 Sigma, Italy) and a control exposed to UVA/B radiation (untreated cells but exposed to UVA/B radiation) and the primary and oxidative DNA fragmentation damage was studied. After exposure, cells were washed twice with 3 mL of PBS, detached with 500 μL per well of trypsin (Invitrogen, Italy) and harvested with 2 mL per well of complete culture medium. The cells were counted and 30 000 cells were included in the second layer of each comet assay slide previously prepared. The first layer consisted of 0.5% (w/v) normal melting point agarose and the second and third layers consisted of 0.5% (w/v) low melting point agarose, (Sigma, Italy). Three slides were prepared for each control and treatment group; one slide was treated with enzyme buffer alone (as a control), the second one was treated with the *E. coli* Endonuclease III (Endo III) enzyme (Tema Ricerca, Italy), and the third one was treated with the *E. coli* formamidopyrimidine DNA-glycosylase (Fpg) enzyme (Tema Ricerca, Italy).

After the solidification of the agarose, the cover slips were removed and the slides were immersed for 1 h at 4 °C in a cold freshly prepared lysis solution (2.5 M NaCl, 100 mM Na_2EDTA, 10 mM Tris, pH 10, containing 1% (v/v) Triton X-100 and 10% (v/v) dimethylsulfoxide, Sigma-Aldrich, Italy). After lysis, the slides were washed with enzyme buffer (100 mM KCl, 10 mM Na_2EDTA, 10 mM HEPES in Milli-Q water for Endo III and with the addition of 0.1 mg mL^{-1} bovine serum albumin for Fpg, both adjusted to pH 7.4) for 15 min at 4 °C, treated with 100 μL of enzyme buffer alone, Endo III or Fpg, covered with a cover slip and put in a moist box at 37 °C for 45 min for enzyme buffer alone and the Endo III enzyme or 30 min for the Fpg enzyme. The slides were placed in an horizontal gel electrophoresis tank filled with electrophoresis cold buffer of 0.3 M NaOH, 1 mM Na_2EDTA for 40 min. Electrophoresis was then carried out at 25 V and approximately 300 mA for 30 min at 4 °C.

After the electrophoresis the slides were washed twice for 5 min with neutralizing buffer (0.4 M Tris, pH 7.5), fixed with absolute ethanol (Carlo-Erba, Italy) for 3 min and stained with 50 μL ethidium bromide (0.4 μM mL^{-1}, Sigma-Aldrich) before the analysis.

The analysis was made using the Komet 6 Image Analysis System (Kinetic Imaging Ltd, Liverpool, UK) fitted with a fluorescence microscope (Olympus, Italy) with the following settings: magnification 40×, wide band excitation filter 480–550 nm and barrier filter 590 nm.

The data are expressed as the median of at least 3 experiments (100 cells per run counted) with DNA (% in tail) and the statistically significant difference of the treatment versus the corre-sponding controls, was calculated by the one-way ANOVA analysis GraphPadPrism4 statistical so ware, GraphPad Inc., CA, USA.

5 Conclusions

The data herein presented suggest that the acute cytotoxic and genotoxic effects elicited by sun-light activated TiO_2 toward human keratinocytes are related to the direct oxidative damage triggered by the release of singlet oxygen by the TiO_2 nano-particles. This finding contributes to the knowledge of robust structure–activity relationships (SAR) that can be used for the safer design of TiO_2 nanopowders.

Acknowledgements

This research has been carried out with the financial support of the University of Torino (Progetti di Ricerca finanziati ex 60%-2012) project title: “Integrated chemical tests for the evaluation of the oxidative potential of nanopowders”.

Notes and references

1 G. Oberdorster, J. Intern. Med., 2010, 267, 89.
2 K. Savolainen, H. Alenius, H. Norppa, L. Pylkkanen, T. Tuomi and G. Kasper, Toxicology, 2010, 269, 92.
3 F. Schrurs and D. Lison, Nat. Nanotechnol., 2012, 7, 546.
4 A. Pietroiusti, Nanoscale, 2012, 4, 1231.
5 N. Serpone, D. Dondi and A. Albini, Inorg. Chim. Acta, 2007, 360, 794.
6 J. Nohynek, E. Antignac, T. Re and H. Toutain, Toxicol. Appl. Pharmacol., 2010, 243, 239.
7 M. E. Burnett and S. Q. Wang, Photodermatol., Photoimmunol. Photomed., 2011, 27, 58.
8 J. M. Davis, T. C. Long, J. A. Shatkin, A. Wang, J. A. Graham, M. Gwinn and B. Ranalli, Photocatalysis: Fundamentals and Applications, Wiley & Sons, Chichester, U.K., 1989.
9 T. Finkel and N. J. Holbrook, Nature, 2000, 408, 239.
10 M. L. Circu and T. Y. Aw, Free Radical Biol. Med., 2010, 48, 749.
11 S. Singh, T. Shi, R. Duffin, C. Albrecht, D. van Berlo, D. Hoehr, B. Fubini, G. Martra, I. Fenoglio, P. J. A. Borm and R. P. F. Schins, Toxicol. Appl. Pharmacol., 2007, 222, 141.
12 M. Simon, P. Barberet, M.-H. Delville, P. Moretto and H. Seznec, Nanotoxicology, 2011, 5, 125.
13 R. K. Shukla, V. Sharma, A. K. Pandey, S. Singh, S. Sultana and A. Dhawan, Toxicol. in Vitro, 2011, 25, 231.
14 R. K. Shukla, A. Kumar, D. Gurbani, A. K. Pandey, S. Singh and A. Dhawan, Nanotoxicology, 2013, 7, 48.
15 Y. Zhao, J. L. C. Howe, Z. Yu, D. Tai Leong, J. J. H. Chu, J. S. C. Loo and K. W. Ng, Small, 2013, 9, 387.
16 R. X. Cai, Y. Kubota, T. Shuin, H. Sakai, K. Hashimoto and A. Fujishima, Cancer Res., 1992, 52, 2346.
17 R. Dunford, A. Salinaro, L. Z. Cai, N. Serpone, S. Horikoshi, H. Hidaka and J. Knowland, FEBS Lett., 1997, 418, 87.
18 Y. Nakagawa, S. Wakuri, K. Sakamoto and N. Tanaka, Mutat. Res., Genet. Toxicol. Environ. Mutagen., 1997, 394, 125.
19 K. Hirakawa, M. Mori, M. Yoshida, S. Oikawa and S. Kawanishi, Free Radical Res., 2004, 38, 439.
20 M. Sayes, R. Wahi, P. A. Kurian, Y. P. Liu, J. L. West, K. D. Ausman, D. B. Warheit and V. L. Colvin, Toxicol. Sci., 2006, 92, 174.
21 C. Xue, J. Wu, F. Lan, W. Liu, X. Yang, F. Zeng and H. Xu, J. Nanosci. Nanotechnol., 2010, 10, 8500.
22 A. Jaeger, D. G. Weiss, L. Jonas and R. Kriehuber, Toxicology, 2012, 296, 27.
23 K. Fujita, M. Horie, H. Kato, S. Endo, M. Suzuki, A. Nakamura, A. Miyauchi, K. Yamamoto, S. Kinugasa, K. Nishio, Y. Yoshidaa, H. Iwahashia and J. Nakanishie, Toxicol. Lett., 2009, 191, 109.
24 T. Ashikaga, M. Wada, H. Kobayashi, M. Mori, Y. Katsumura, H. Fukui, S. Kato, M. Yamaguchi and T. Takamatsu, Mutat. Res., Genet. Toxicol. Environ. Mutagen., 2000, 466, 1.
25 C. A. Rice-Evans, A. T. Diplock and M. C. R. Symons, Techniques in free radical research, Elsevier, Amsterdam, 1991.
26 J. Cadet, T. Douki and J.-L. Ravanat, Acc. Chem. Res., 2008, 41, 1075.
27 H. Tahiri, N. Serpone and R. Le van Mao, J. Photochem. Photobiol., A, 1996, 93, 199.
28 K. Gerloff, I. Fenoglio, E. Carella, J. Kolling, C. Albrecht, A. W. Boots, I. Foerster and R. P. F. Schins, Chem. Res. Toxicol., 2012, 25, 646.
29 S. Livraghi, I. Corazzari, M. C. Paganini, G. Ceccone, E. Giamello, B. Fubini and I. Fenoglio, Chem. Commun., 2010, 46, 8478.
30 I. Corazzari, S. Livraghi, S. Ferrero, E. Giamello, B. Fubini and I. Fenoglio, J. Mater. Chem., 2012, 22, 19105.
31 O. Carp, C. L. Huisman and A. Reller, Prog. Solid State Chem., 2004, 32, 33.
32 A. Fujishima, X. Zhang and D. A. Tryk, Surf. Sci. Rep., 2008, 63, 515.
33 Q. Jin, M. Fujishima and H. Tada, J. Phys. Chem. C, 2011, 115, 6478.
34 H. Yu, H. Irie, Y. Shimodaira, Y. Hosogi, Y. Kuroda, M. Miyauchi and K. Hashimoto, J. Phys. Chem. C, 2010, 114, 16481.
35 J. C. Colmenares, M. A. Aramendia, A. Marinas, J. M. Marinas and F. J. Urbano, Appl. Catal., A, 2006, 306, 120.
36 L. Wen, B. Liu, X. Zhao, K. Nakata, T. Murakami and A. Fujishima, Int. J. Photoenergy, 2012, 1.
37 J. Yu, Q. Xiang and M. Zhou, Appl. Catal., B, 2009, 90, 595.
38 S. Rehman, R. Ullah, A. M. Butt and N. D. Gohar, J. Hazard. Mater., 2009, 170, 560.
39 C. F`abrega, T. Andreu, A. Cabot and J. R. Morante, J. Photochem. Photobiol., A, 2010, 211, 170.
40 G. Oberdorster, A. Maynard, K. Donaldson, V. Castranova, J. Fitzpatrick, K. Ausman, J. Carter, B. Karn, W. Kreyling, D. Lai, S. Olin, N. Monteiro-Riviere, D. Warheit and H. Yang, Part. Fibre Toxicol., 2005, 2, 8.
41 I. Fenoglio, G. Greco, S. Livraghi and B. Fubini, Chem.–Eur.J., 2009, 15, 4614.
42 I. Fenoglio, B. Fubini, E. M. Ghibaudi and F. Turci, Adv. Drug Delivery Rev., 2011, 63, 1186.
43 S. Shari , S. Behzadi, S. Laurent, M. L. Forrest, P. Stroeve and M. Mahmoudi, Chem. Soc. Rev., 2012, 41, 2323.
44 L. Cromi`eres, V. Moulin, B. Fourest and E. Giffaut, Colloids Surf., A, 2002, 202, 101.
45 V. Brezova, S. Gabcova, D. Dvoranova and A. Stasko, J. Photochem. Photobiol., B, 2005, 79, 121.
46 Z. Wang, W. Ma, C. Chen, H. Ji and J. Zhaoa, Chem. Eng. J., 2011, 170, 353.
47 T. Daimon, T. Hirakawa, M. Kitazawa, J. Suetake and Y. Nosaka, Appl. Catal., A, 2008, 340, 169–175.
48 R. Konaka, E. Kasahara, W. C. Dunlap, Y. Yamamoto, K. C. Chien and M. Inoue, Free Radical Biol. Med., 1999, 27, 294.
49 J. I. Kim, J. H. Lee, D. S. Choi, B. M. Won, M. Y. Jung and J. Park, J. Food Sci., 2009, 74, C362.
50 E. L. Clennan and A. Pace, Tetrahedron, 2005, 61, 6665.
51 X. Yang and Y. Wang, Build. Environ., 2008, 43, 253.
52 C. Pfannschmidt and J. Langowski, J. Mol. Biol., 1998, 275, 601.
53 A. I. Kontos, A. G. Kontos, D. S. Tsoukleris, G. D. Vlachos and P. Falaras, Thin Solid Films, 2007, 515, 7370.

54 H. L. Karlsson, Anal. Bioanal. Chem., 2010, 398, 651.
55 G. J. Nohynek, J. Lademann, C. Ribaud and M. S. Roberts, Crit. Rev. Toxicol., 2007, 37, 251.
56 M. Loden, H. Beitner, H. Gonzalez, D. W. Edstrom, U. Akerstrom, J. Austad, I. Buraczewska-Norin, M. Matsson and H. C. Wulf, Br. J. Dermatol., 2011, 165, 255.
57 J. Rockler, M. Oelgemoeller, S. Robertson and B. D. Glass, J. Photochem. Photobiol., C, 2012, 13, 91.
58 S. Dussert, E. Gooris and J. Hemmerle, Int. J. Cosmet. Sci., 1997, 19, 119.
59 O. Gamer, E. Leibold and B. van Ravenzwaay, Toxicol. in Vitro, 2006, 20, 301.
60 A. Mavon, C. Miquel, O. Lejeune, B. Payre and P. Moretto, Skin Pharmacol. Physiol., 2007, 20, 10.
61 T. Pinheiro, J. Pallon, L. C. Alves, A. Verissimo, P. Filipe, J. N. Silva and R. Silva, Nucl. Instrum. Methods Phys. Res., Sect. B, 2007, 260, 119.
62 F. M. Christensen, H. J. Johnston, V. Stone, R. J. Aitken, S. Hankin, S. Peters and K. Aschberger, Nanotoxicology, 2011, 5, 110.
63 N. A. Monteiro-Riviere, K. Wiench, R. Landsiedel, S. Schulte, A. O. Inman and J. E. Riviere, Toxicol. Sci., 2011, 123, 264.
64 Nanomaterial Case Studies: Nanoscale Titanium Dioxide in Water Treatment and in Topical Sunscreen National Centre for Environmental Assessment, RTP Division Office of Research and Development U.S. Environmental Protection Agency, 2010, EPA/600/R-09/057F.
65 R. Landsiedel, L. Ma-Hock, B. van Ravenzwaay, M. Schulz, K. Wiench, S. Champ, S. Schulte, W. Wohlleben and F. Oesch, Nanotoxicology, 2010, 4, 364.
66 C. Lee, H. Kim, Y. Cho and W. I. Lee, J. Mater. Chem., 2007, 17, 2648.
67 E. Carlotti, E. Ugazio, S. Sapino, I. Fenoglio, G. Greco and B. Fubini, Free Radical Res., 2009, 43, 312.
68 L. Tiano, T. Armeni, E. Venditti, G. Barucca, L. Mincarelli and E. Damiani, Free Radical Biol. Med., 2010, 49, 408.
69 M. Buchalska, G. Kras, M. Oszajca, W. Lasocha and W. Macyk, J. Photochem. Photobiol., A, 2010, 213, 158.
70 M. G. Sacco, F. Pariselli and D. A. Rembges, Fresenius Environ. Bull., 2010, 19, 1537–1543.

Fenoglio I. et al. Singlet oxygen plays a key role in the toxicity and DNA damage of nanometric TiO_2 to human keratinocytes

Supporting Information

1.Crystalline phase (XRD)

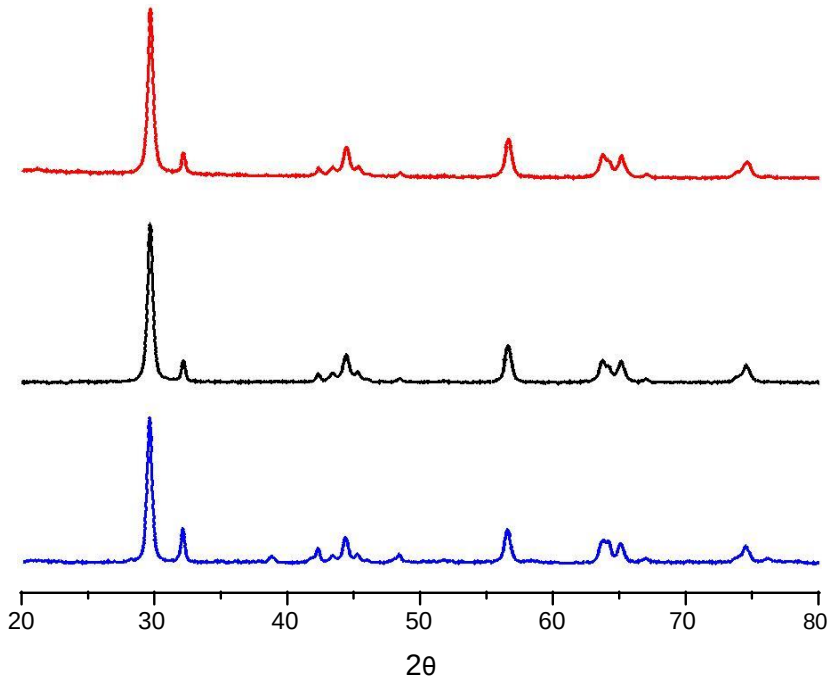

XRD diffraction patterns of pristine and modified TiO_2. $T_{A/R}$ (blue), $T_{A/R}$-C (black), $T_{A/R}$-Fe (red).

2. UV-Vis shielding capacity

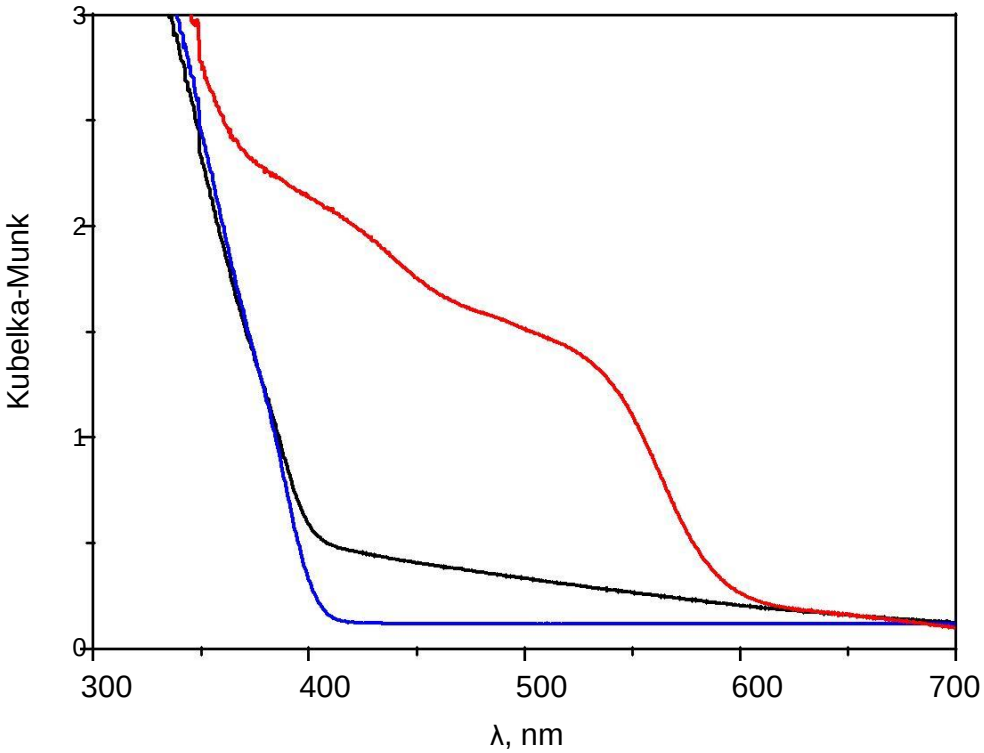

Diffuse reflectance (DR) UV-Vis spectra (processed by using the Kubelka–Munk function). $T_{A/R}$ (blue), $T_{A/R}$-C (black), $T_{A/R}$-Fe (red).

3. ζ **potential**

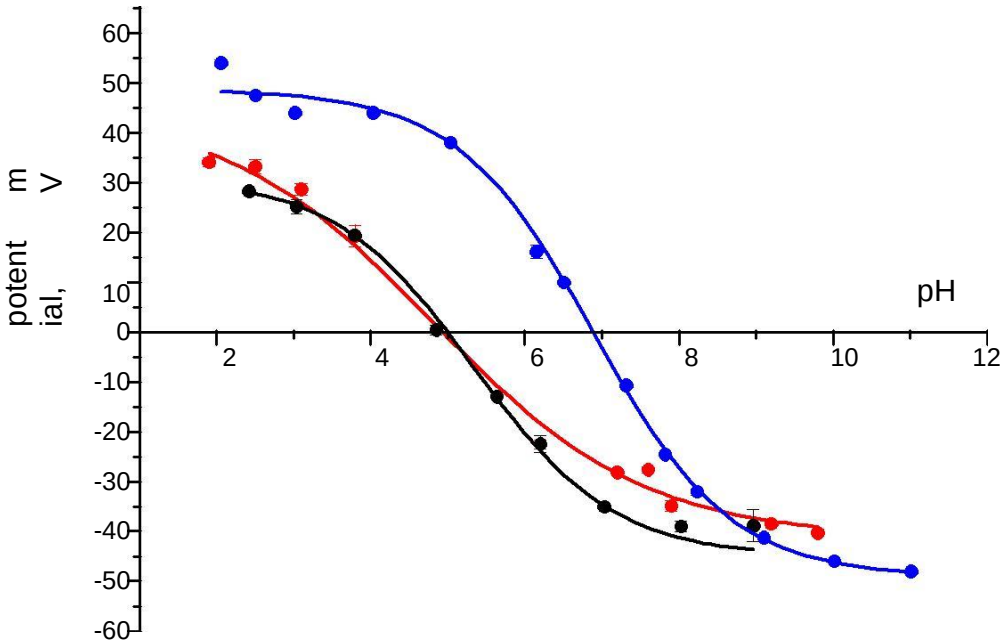

ζpotential as a function of pH for $T_{A/R}$ (blue), $T_{A/R}$ –C (black) and $T_{A/R}$ –Fe (dark red) recorded in water.

4. Particle size

Sample	Conditions	Water		Serum free cell media		Cell media	
		mean diameter (nm)	PDI	mean diameter (nm)	PDI	mean diameter (nm)	PDI
$T_{A/R}$	0 min	89	1.60	245	2.12	178	3.5
	15 min light	119	1.64	471	1.68	343	2.79
	2h dark	104	2.13	310	2.04	184	3.03
$T_{A/R}$-Fe	0 min	108	1.70	252	6.50	247	1.52
	15 min light	130	1.52	747	10.03	320	2.02
	2h dark	105	1.40	320	3.35	190	1.61
$T_{A/R}$-C	0 min	92	3.44	192	2.05	250	4.25
	15 min light	121	2.44	491	2.09	361	3.48
	2h dark	79.5	2.56	250	3.60	248	5.52

Size and polydispersity index of the particles evaluated by centrifugal sedimentation (CS).

5. UVA/B irradiation system in cellular experiments

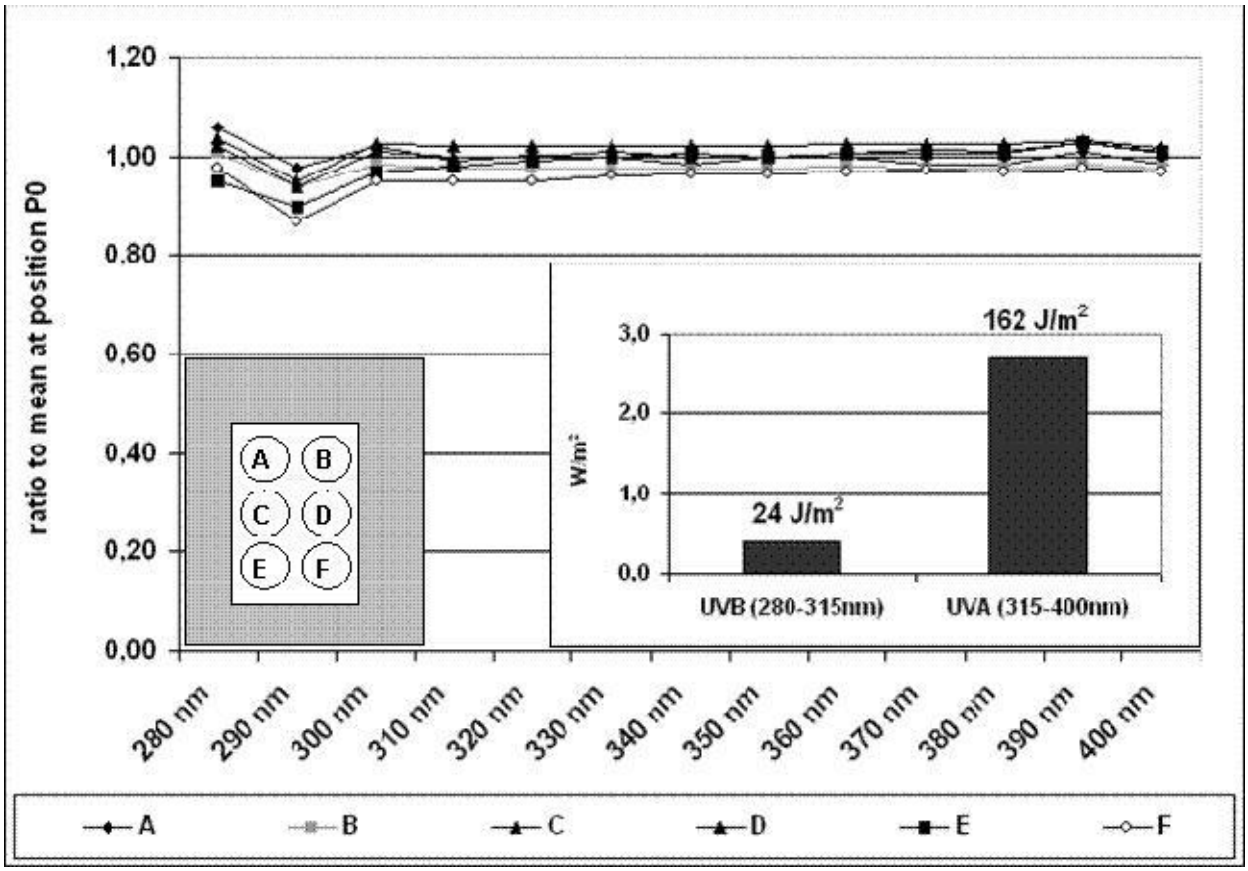

UV radiation measurements demonstrating the homogeneity over all positions of the 6 well plates at a well defined distance from the Ultralux lamp. Adapted from Sacco et al. 2010.